THE JOURNAL OF BIOLOGICAL CHEMISTRY VOL. 288, NO. 14, pp. 9593–9601, April 5, 2013
© 2013 by The American Society for Biochemistry and Molecular Biology, Inc. Published in the U.S.A.

Glutamate Acts as a Partial Inverse Agonist to Metabotropic Glutamate Receptor with a Single Amino Acid Mutation in the Transmembrane Domain*

Received for publication, November 19, 2012, and in revised form, February 15, 2013 Published, JBC Papers in Press, February 18, 2013, DOI 10.1074/jbc.M112.437780

Masataka Yanagawa, Takahiro Yamashita, and Yoshinori Shichida[1]

From the Department of Biophysics, Graduate School of Science, Kyoto University, Kyoto 606-8502, Japan

Background: Conformational change of transmembrane domain of mGluR upon glutamate binding is unknown.
Results: Moderate steric hindrance between helices VI and VII of mGluR caused constitutive activation and severe steric hindrance caused deactivation.
Conclusion: Proper outward movement of helix VI is a critical determinant of activation of mGluR like rhodopsin.
Significance: Underlying activation mechanism is common across families of GPCRs.

Metabotropic glutamate receptor (mGluR), a prototypical family 3 G protein-coupled receptor (GPCR), has served as a model for studying GPCR dimerization, and growing evidence has revealed that a glutamate-induced dimeric rearrangement promotes activation of the receptor. However, structural information of the seven-transmembrane domain is severely limited, in contrast to the well studied family 1 GPCRs including rhodopsins and adrenergic receptors. Homology modeling of mGluR8 transmembrane domain with rhodopsin as a template suggested the presence of a conserved water-mediated hydrogen-bonding network between helices VI and VII, which presumably constrains the receptor in an inactive conformation. We therefore conducted a mutational analysis to assess structural similarities between mGluR and family 1 GPCRs. Mutational experiments confirmed that the disruption of the hydrogen-bonding network by T789Y$^{6.43}$ mutation induced high constitutive activity. Unexpectedly, this high constitutive activity was suppressed by glutamate, the natural agonist ligand, indicating that glutamate acts as a partial inverse agonist to this mutant. Fluorescence energy transfer analysis of T789Y$^{6.43}$ suggested that the glutamate-induced reduction of the activity originated not from the dimeric rearrangement but from conformational changes within each protomer. Double mutational analysis showed that the specific interaction between Tyr-789$^{6.43}$ and Gly-831$^{7.45}$ in T789Y$^{6.43}$ mutant was important for this phenotype. Therefore, the present study is consistent with the notion that the metabotropic glutamate receptor shares a common activation mechanism with family 1 GPCRs, where rearrangement between helices VI and VII causes the active state formation.

G protein-coupled receptors (GPCRs)[2] constitute the largest superfamily of membrane proteins that translate various extracellular signals into an intracellular message via activation of trimeric G proteins. Because GPCRs are major drug targets, their structure-function relationship is a key issue for novel drug design and elucidation of the mechanism of drug action. All GPCRs have a seven-transmembrane domain (TMD) and are classified into several families based on sequence similarity (1). Recently, the crystal structures of active states of family 1 GPCRs including rhodopsin and adrenergic receptor were published (2, 3), providing important insights into conformational changes in the cytoplasmic side of the TMD. Specifically, it can be speculated that remarkable changes such as the extension of helix V and the outward movement of helix VI are essential for exposing the G protein binding sites. These structural changes are accompanied by the reorganization of hydrogen-bonding networks (HBNs) among helices III, V, VI, and VII including E(D)RY and NP*XX*Y motifs, both of which are highly conserved in family 1 GPCRs. Despite many fundamental advances made in family 1 GPCRs, it is still unclear how common this activation mechanism is among other families. Therefore, in the present study, we examined whether or not similar structural requirements are needed for the active state formation of metabotropic glutamate receptor (mGluR), a prototypical family 3 GPCR.

Homology modeling of the resting state of mGluR8 constructed based on the rhodopsin template predicted the presence of a structural water-mediated HBN between helices VI and VII (Fig. 1*a*). In family 1 GPCRs, this HBN is considered essential to keep the receptor inactive (4, 5), and mutations at these loci result in elevated constitutive activity (6). We have previously reported a constitutively active mutation, T789A$^{6.43}$ in mGluR8 (7), which is located in the HBN according to our homology model (superscript numbers represent the Ballesteros and Weinstein nomenclature for GPCRs (8)). The

* This work was supported by the Ministry of Education, Culture, Sports, Science, and Technology (MEXT), Japan, Grants-in-aid for Scientific Research 20227002 and 21026019, and the Global Center of Excellence Program "Formation of a Strategic Base for Biodiversity and Evolutionary Research: from Genome to Ecosystem" (Program A06), and Japan Society for the Promotion of Science (JSPS) Research Fellowship for Young Scientists 08J01259.

[1] To whom correspondence should be addressed. Tel.: 81-75-753-4213; Fax: 81-75-753-4210; E-mail: shichida@rh.biophys.kyoto-u.ac.jp.

[2] The abbreviations used are: GPCR, G protein-coupled receptor; L-AP4, L-(+)-2-amino-4-phosphonobutyric acid; GTPγS, guanosine 5′-3-*O*-(thio)triphosphate; HBN, hydrogen-bonding network; LY341495, (2*S*)-2-amino-2-[(1*S*,2*S*)-2-carboxycycloprop-1-yl]-3-(xanth-9-yl) propanoic acid; mGluR, metabotropic glutamate receptor; TMD, transmembrane domain.

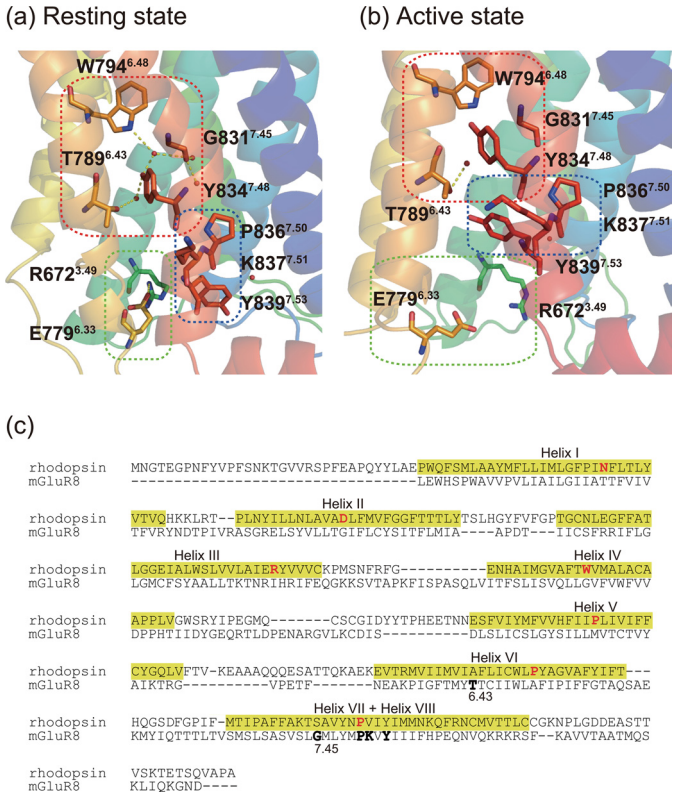

FIGURE 1. **Homology models of TMD of mGluR8.** *a* and *b*, homology models of the resting state (*a*) and the active state (*b*) of mGluR8 were constructed based on the crystal structures of the resting state (1U19) and the active state (3PXO) of bovine rhodopsin. The seven helices are represented in different colors (*blue* to *red*). The water-mediated HBN is indicated by a *red dashed frame*. The water molecules were fixed at the corresponding positions to the template structures of bovine rhodopsin. The highly conserved *X*PK*X*Y motif is indicated by a *blue dashed frame*. A *green dashed frame* indicates the ionic lock between helices III and VI, which was also predicted in $GABA_B$ receptor (28). *Dashed yellow lines* indicate possible hydrogen bonds which are connected by two hydrophilic atoms within 4 Å. *c*, alignment of amino acid sequences of bovine rhodopsin and mGluR8. Transmembrane helices of bovine rhodopsin are *highlighted* in *yellow*. The superconserved residues in family 1 GPCRs on each helix are shown as *red bold letters*. Thr-$789^{6.43}$, Gly-$831^{7.45}$, and *X*PK*X*Y motif in mGluR8 are shown in *black bold letters*.

increased constitutive activity by the disruption of the HBN suggests a common activation mechanism between family 1 and family 3 GPCRs. Therefore, in the present study, we performed comprehensive mutation analysis at this locus to further investigate the role of this region. As a result, we identified an unexpected unique phenotype in $T789Y^{6.43}$. Our results show that the high constitutive activity of $T789Y^{6.43}$ was suppressed by glutamate binding; that is, glutamate acts as a partial inverse agonist on $T789Y^{6.43}$. Further analysis with double mutations suggested that this unique phenotype can be attributed to a specific interaction between Tyr-$789^{6.43}$ and Gly-$831^{7.45}$ in $T789Y^{6.43}$ mutant, which is consistent with a conserved activation mechanism between helices VI and VII in family 1 and family 3 GPCRs.

Several studies indicate that dimeric rearrangement of TMDs following the conformational change of the extracellular ligand binding domain is important for the active state formation of mGluRs (9–14). Therefore, we performed fluorescence resonance energy transfer (FRET) analysis to test whether $T789Y^{6.43}$ affected the glutamate-induced dimeric rearrangement of TMD. The results showed that $T789Y^{6.43}$ mutant exhibited dimeric rearrangement quite similar to wild-type receptor, suggesting that the unique phenotype in the mutant originated not from different dimeric rearrangement but from a characteristic state of helix VI within each protomer. Taken together, we discuss the model that a proper positional relationship between helices VI and VII within each protomer is a major determinant of the activation of mGluR.

EXPERIMENTAL PROCEDURES

Materials—[^{3}H]LY341495 (1.28 terabecquerels/mmol) and L-AP4 were purchased from Tocris Cookson. [^{35}S]GTPγS (37 terabecquerels/mmol) were from PerkinElmer Life Sciences. Monoclonal anti-GFP and clone GFP-20 mouse ascites fluid were from Sigma.

Construction of mGluR Mutants—Site-directed mutagenesis was performed by using the QuikChange kit (Agilent Technologies). The mCerulean (15) or Venus (16) coding region (Val-2 through Leu-237) was inserted into each intracellular loop region of Pro-774 through Glu-775 of mGluR8 by an In-Fusion PCR cloning kit (Clontech). To detect the expression of mGluR8 by Western blotting analysis, the cDNAs of mGluR8 were tagged with the epitope sequence of the anti-bovine rhodopsin monoclonal antibody Rho1D4 at the C terminus. The wild-type and mutant cDNAs of mGluR8 were introduced into the mammalian expression vector pcDNA3.1 (Invitrogen) or pCAGGS (17).

Preparation of mGluR Wild Type and Mutants—Expression of mGluRs in HEK293S cells was performed by the methods reported previously (13). HEK293S cells were grown to ~40% confluence in DMEM/F12 supplemented with 10% fetal bovine serum and were transfected with wild-type or mutant mGluR8 plasmid DNA (10 μg/100-mm dish) using the calcium-phosphate method. The cells were collected by centrifugation 48 h after transfection. The cell membranes were homogenized in 50% sucrose in buffer A (50 mM HEPES (pH 6.5) and 140 mM NaCl) prior to centrifugation. The supernatant was diluted in 2 volumes of buffer A and recentrifuged. Membrane pellets were suspended in buffer B (50 mM HEPES (pH 8.0), 140 mM NaCl, and 3 mM $MgCl_2$) for the ligand binding assay and the GTPγS binding assay. For the FRET analysis, the membrane pellets were washed three times for over 2 h with low salt buffer (5 mM HEPES (pH 8.0) and 0.3 mM EDTA) to reduce autofluorescence derived from cell surface proteins.

Ligand Binding Assay of mGluR8—The ligand binding assay was performed according to our previous report (7). Displacement by L-AP4 or glutamate of [^{3}H]LY341495 binding to the cell membranes expressing mGluR8 was measured at room temperature. A mixture of membranes (30 μg of total protein), 100 nM [^{3}H]LY341495, and 0–100 μM L-AP4 in buffer B or 0–10 mM glutamate in buffer C (10 mM HEPES (pH 7.5) and 140 mM NaCl, 4 mM KOH, 1 mM $MgCl_2$, and 1.5 mM $CaCl_2$) was incubated for 30 min (final assay volume, 20 μl). After incubation, bound and free radioligands were separated by centrifugation. The membrane pellets were washed with buffer B or C and solubilized in 1 M NaOH. The specific binding, defined using 1 mM L-AP4 or 10 mM glutamate as displacer, was ~93% of total binding estimated using 100 nM [^{3}H]LY341495 and 30

μg of tissue protein. Protein concentration in the membranes was determined by the Bradford method. Competition binding curves were fitted to the one-site binding model: $y = (\text{Max-Basal})/(1 + x/\text{IC}_{50}) + \text{Basal}$.

GTPγS Binding Assay of mGluR8—The assay of G protein activation by mGluR8 was carried out according to our previous report (18). The mGluR8-containing membranes (final concentration, 2 nM) after sucrose flotation were suspended in 0.03% dodecylmaltoside in buffer D (50 mM HEPES (pH 7.2), 140 mM NaCl, and 3 mM $MgCl_2$) and preincubated with G_o-type G protein (final concentration, 200 nM) purified from pig cerebral cortex and the agonist L-AP4 or glutamate. After preincubation for 30 min at 10 °C, the GDP/GTPγS exchange reaction was started by adding GTPγS solution. The assay mixture (20 μl) consisted of 50 mM HEPES (pH 7.2), 140 mM NaCl, 5 mM $MgCl_2$, 0.015% dodecylmaltoside, 0.03% sodium cholate, 0.8 mg/ml L-α-phosphatidylcholine, 0.1 μM GTPγS, and 3 μM GDP. After incubation for 3 min, the reaction was terminated by adding stop solution (200 μl: 20 mM tris(hydroxymethyl)-aminomethane (pH 7.4), 100 mM NaCl, 25 mM $MgCl_2$, 0.1 μM GTPγS, and 3 μM GDP) and immediately filtering the sample through a nitrocellulose membrane to trap [^{35}S]GTPγS bound to G proteins.

Fluorescence Microscopy—The cellular expression of fluorescence protein-fused mGluR mutants was observed in phosphate-buffered saline on a Nikon Eclipse TE300 inverted microscope with a TE-FM fluorescence attachment as reported in Ref. 13. A high pressure mercury lamp (HB 10103AF) with a 450–490-nm band pass filter was used for the excitation of fluorescence proteins, and fluorescence was detected with a 505-nm dichroic mirror and a 520-nm longpass filter (Nikon B-2A filter set).

FRET Analysis of mGluRs—The FRET analysis was performed according to our previous report (13). Briefly, fluorescence spectra from Cerulean- and Venus-fused mGluRs were recorded at 20 °C with an RF-5300PC spectrofluorophotometer (Shimadzu). The membrane pellets prepared as described above were resuspended in buffer C and were excited at 433 nm for Cerulean or 500 nm for Venus. To block the scattering, cutoff filters (Y-45 for 433 nm excitation and Y-51 for 500 nm excitation) were placed in front of the detector. Autofluorescence spectra from the membranes containing wild-type mGluRs were also recorded in the same conditions as the base line. We estimated the FRET efficiency and the amount of Cerulean- or Venus-fused mGluRs in co-expressing samples from the base line-corrected fluorescence spectra by "spectra FRET" analysis as described in a previous report (13).

Homology Modeling—Homology modeling of TMD of mGluR8 was performed by using Modeller (19). We used the crystal structures of bovine rhodopsin (Protein Data Bank code: 1U19 (20) and 3PXO (2)) as template for homology modeling in the resting and active states. The alignment between mGluR8 and rhodopsin was constructed in accordance to previous reports (21–25), in which the binding pockets of allosteric modulators of family 3 GPCRs were successfully predicted using the molecular modeling based on the crystal structure of bovine rhodopsin (Fig. 1*c*). The alignment and the methodology for homology modeling in the present study were identical to the recently published report of mGluR2 that investigated the structural properties of helix VIII using the homology modeling and molecular dynamics simulations (25). The created model was depicted using PyMOL (26).

RESULTS

Homology Modeling of mGluR8—Although sequence similarity between family 1 and family 3 GPCRs is very low, several conserved residues can serve as landmarks for sequence alignment (27). Homology modeling of family 3 GPCRs based on the crystal structure of bovine rhodopsin has been successful for predicting binding sites of allosteric ligands (21–25). In the present study, we created a homology model of the TMD of mGluR8 in its resting and active states to investigate the activation mechanism (see "Experimental Procedures"). The resting state model predicts an ionic lock between Arg-672$^{3.49}$ and Glu-779$^{6.33}$ (Fig. 1*a*), which is consistent with previous mutation analysis of $GABA_B$ receptor (28). Moreover, a structural water-mediated HBN between helices VI and VII was predicted in the vicinity of highly conserved *X*PK*X*Y motif that corresponds to the NP*XX*Y motif in the cytoplasmic end of helix VII in family 1 receptors (Fig. 1*a*). However, these interactions disappeared in the active state model along with the outward movement of helix VI (Fig. 1*b*). Consequently, Arg-672$^{3.49}$ was displaced toward the cytoplasmic space, which is considered essential for interaction with G protein (28), similar to Arg$^{3.50}$ in the ERY motif of family 1 receptors (2, 3). These models suggest that, like rhodopsin, reorganization of HBNs controls the activation of mGluR, even though sequence similarity is very low across the families.

Characterization of mGluR8 Thr-789$^{6.43}$ Mutants—The homology model suggested that Thr-789$^{6.43}$ is involved in the structural water-mediated HBN between helices VI and VII (Fig. 1*a*). Our previous study showed that the mutation at Thr-789$^{6.43}$, which is well conserved among all of the eight human mGluR subtypes, elevated the constitutive activity (7). To further investigate the role of this residue, we performed a comprehensive mutational analysis of this constitutively active mutation site. We constructed all 19 mutants at Thr-789$^{6.43}$ and expressed them in HEK293 cells. The expression level of wild type and the mutants was determined by a ligand binding assay using a membrane preparation. Substitutions with charged amino acid residues (Asp, Glu, His, Lys, and Arg) or Asn resulted in substantial decrease of expression level (Table 1).

G protein activation ability of the mutants whose expression level was >40% of wild type was measured by GTPγS binding assay with or without agonist L-AP4. The constitutive activity was positively correlated with the difference in side chain volume from threonine ($r = 0.85$, $p < 0.01$) in all of the mutants except for T789W$^{6.43}$ (Fig. 2*a*). Thus, a large change in the side chain volume at this locus increased the constitutive activity. Additionally, when the substituted residue was smaller than threonine, all four mutants showed significant elevation (~1.5-fold of wild type) of the agonist (L-AP4)-dependent activity (Fig. 2*b*). However, when the substituted residue was larger than threonine, the agonist-dependent activity was not correlated with side chain volume of the residue (Fig. 2*c*). Among these

TABLE 1

Relative expression level of the mutants of mGluR8

Relative expression level of the mutants of mGluR8 was estimated using the ligand binding assay (see "Experimental Procedures"). The absolute amount of expression of wild type was 63 pmol/mg of total protein. Each amount of expression is expressed as the mean ± S.D. of two independent experiments done in duplicate.

Position mGluR8	TM6 (6.43) mean ± S.D.	Position mGluR8	TM7 mean ± S.D.	Position mGluR8	TM7+T789Y$^{6.43}$ mean ± S.D.
WT	1.00				
T789G	1.00 ± 0.07	A826S$^{7.40}$	1.02 ± 0.08	A826S/T789Y	0.97 ± 0.08
T789A	1.04 ± 0.01	S827A$^{7.41}$	1.06 ± 0.07	S827A/T789Y	0.66 ± 0.05
T789S	1.04 ± 0.02	V828A$^{7.42}$	1.11 ± 0.07	V828A/T789Y	0.93 ± 0.04
T789C	0.99 ± 0.03	S829A$^{7.43}$	1.26 ± 0.15	S829A/T789Y	1.15 ± 0.12
T789P	1.03 ± 0.05	L830A$^{7.44}$	0.12 ± 0.01	L830A/T789Y	0.02 ± 0.00
T789D	0.04 ± 0.00	G831A$^{7.45}$	1.05 ± 0.09	G831A/T789Y	0.96 ± 0.07
T789N	0.02 ± 0.00	M832A$^{7.46}$	1.03 ± 0.04	M832A/T789Y	0.93 ± 0.10
T789V	1.07 ± 0.05	L833A$^{7.47}$	0.08 ± 0.00	L833A/T789Y	0.04 ± 0.00
T789E	0.22 ± 0.12	Y834A$^{7.48}$	0.77 ± 0.05	Y834A/T789Y	0.80 ± 0.05
T789Q	1.02 ± 0.11	M835A$^{7.49}$	0.84 ± 0.05	M835A/T789Y	0.96 ± 0.04
T789I	1.02 ± 0.07	P836A$^{7.50}$	0.76 ± 0.07	P836A/T789Y	0.88 ± 0.05
T789L	1.04 ± 0.03	K837A$^{7.51}$	0.78 ± 0.06	K837A/T789Y	0.65 ± 0.03
T789M	0.87 ± 0.11	V838A$^{7.52}$	0.88 ± 0.01	V838A/T789Y	0.94 ± 0.02
T789H	0.32 ± 0.01	Y839A$^{7.53}$	0.81 ± 0.09	Y839A/T789F	1.00 ± 0.07
T789K	0.47 ± 0.02	I840A$^{7.54}$	0.95 ± 0.11	I840A/T789Y	0.87 ± 0.09
T789F	1.07 ± 0.04				
T789R	0.27 ± 0.09				
T789Y	0.98 ± 0.03				
T789W	0.97 ± 0.02				

mutants, T789Y$^{6.43}$ showed a unique phenotype. In addition to having the highest constitutive activity, its constitutive activity was partially suppressed by the addition of agonist L-AP4 (Fig. 2*c*); that is, L-AP4 acted as a partial inverse agonist on T789Y$^{6.43}$.

FRET Analysis on T789Y$^{6.43}$—Previous studies have shown that the intersubunit rearrangement of mGluR dimer can be estimated by FRET analysis using two GFP variants (12–14). Thus, we performed FRET analysis on T789Y$^{6.43}$ mutant to test whether or not the "agonist"-induced reduction of the activity originated from alterations of the intersubunit rearrangement of mGluR dimer. We inserted the fluorescent protein Cerulean (15) or Venus (16) in the intracellular loop 3 of T789Y$^{6.43}$ mutant and co-expressed them in HEK293 cells. The cell surface expression of Cerulean- or Venus-fused T789Y$^{6.43}$ was monitored by fluorescence microscopy (Fig. 3*a*). The receptor localization was not affected by the T789Y$^{6.43}$ mutation compared with the Cerulean- and Venus-fused wild-type mGluR8 reported previously (13). The amounts of expressed Cerulean- and Venus-fused T789Y$^{6.43}$ were estimated from their emission spectra to be 15.0 ± 0.3 and 14.4 ± 0.6 pmol/mg of total protein, respectively. These values are about half of those of Cerulean- and Venus-fused wild-type mGluR8 (34.4 ± 3.2 and 25.7 ± 1.8 pmol/mg of total protein, respectively) and are enough to measure FRET according to our previous study (13).

Fig. 3*b* shows fluorescence spectra of the membrane preparation containing T789Y$^{6.43}$-Celurean/Venus heterodimer under various concentration of glutamate, which is a natural ligand. We calculated the glutamate-dependent change of FRET efficiency, which reflects the distance between two fluorophores. The glutamate-induced change of FRET efficiency in T789Y$^{6.43}$ was quite similar to that in wild type (Fig. 3*c*). There was no statically significant difference between each point of WT and T789Y$^{6.43}$ in Fig. 3*c* ($p > 0.05$; Student's *t* test, two-tailed). This observation suggests that the agonist-dependent intersubunit rearrangement of mGluR dimer, namely the approximation of two intracellular loop 3s, was maintained in T789Y$^{6.43}$. These results strongly suggested that the mutation T789Y$^{6.43}$ altered not the dimeric rearrangement but the conformation within each protomer. We also analyzed the displacement by glutamate of [^{3}H]LY341495 binding to the membrane containing Cerulean- and Venus-fused T789Y$^{6.43}$ to analyze the affinity to glutamate (Fig. 3*d*). There was no significant difference in K_i values between wild type (55 ± 11 μM) and T789Y$^{6.43}$ (41 ± 3.7 μM). These values were similar to EC_{50} of glutamate-dependent increase of FRET efficiency in wild type (61 ± 11 μM) and T789Y$^{6.43}$ (35 ± 6.8 μM) (Fig. 3*c*), suggesting that the dimeric rearrangement of TMDs is tightly coupled to the glutamate-dependent conformational change of extracellular domains. The partial reduction of the activity of T789Y$^{6.43}$ was also monitored in a glutamate concentration-dependent manner by GTPγS binding assay (Fig. 3*e*).

Homology Modeling of mGluR8 Mutants—We used a homology model of mutants to further explore and analyze the molecular mechanism that allows residue 789$^{6.43}$ to modulate the agonist-dependent increase or decrease of the activity. Homology models of T789Y/F/W$^{6.43}$ based on the resting state of rhodopsin resulted in residue side chains ejected from the helical bundles due to steric hindrance (Fig. 4, *a–c*), which is not likely to occur in the lipid bilayer. However, homology models of T789F/Y$^{6.43}$ based on the active state of rhodopsin showed introduced residues fitted in the space within helical bundles accompanied by the outward movement of helix VI similar to wild type (Fig. 4, *d–f* and *i*). In contrast, the side chain of T789W$^{6.43}$ did not fit within helical bundles even though the space between helices VI and VII was expanded in the active state (Fig. 4, *g* and *i*).

These models are consistent with the results of the mutation analysis as shown in Fig. 2. The positive correlation between the side chain volume and the constitutive activity suggests that a steric hindrance at the microenvironment around position 789$^{6.43}$ destabilized the resting state and induced the shift to the active state (Figs. 2*a* and 4, *a*–c). T789W$^{6.43}$ was a clear exception to the correlation because tryptophan was too large to stabilize not only the resting state but also the active state (Figs. 2*a* and 4, *c*, *h*, and *i*). In T789Y/F$^{6.43}$, the introduced residues fitted

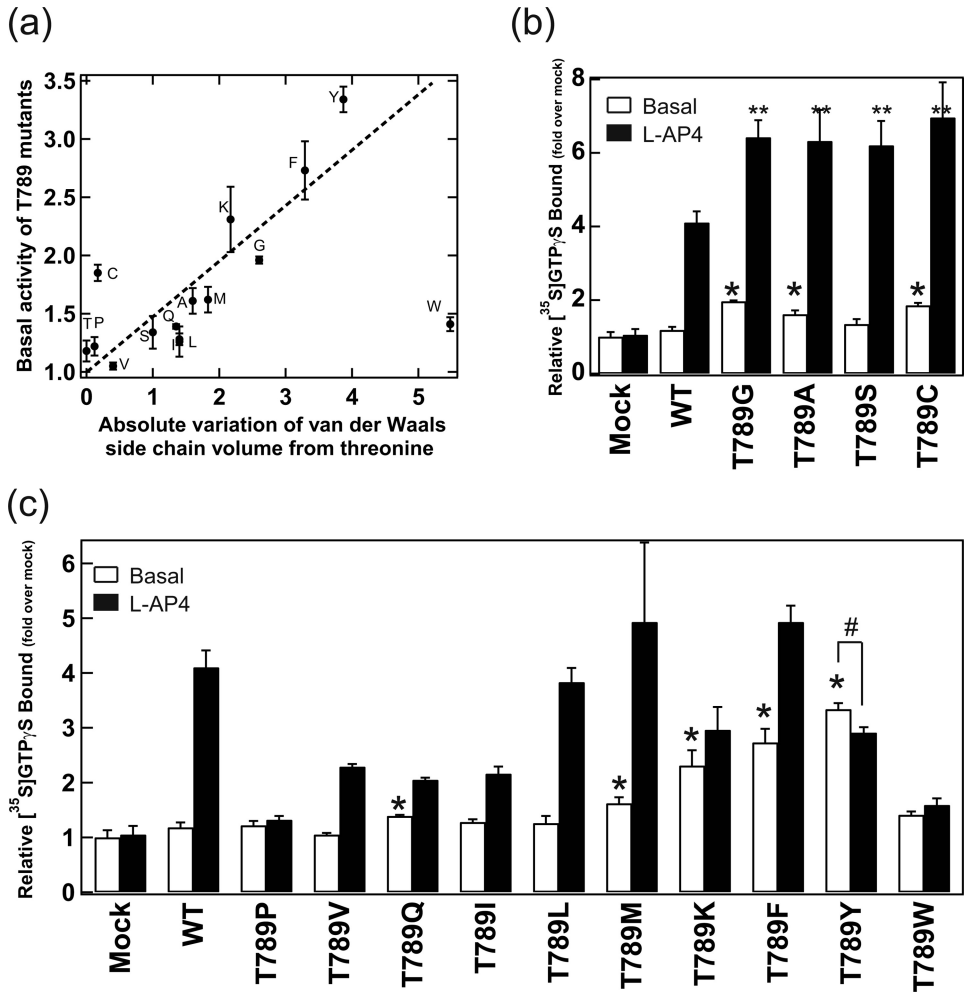

FIGURE 2. **Characterization of the mutations at Thr-789$^{6.43}$ in mGluR8.** *a*, correlation between the constitutive activity of the mutants and the absolute variation of van der Waals side chain volume from threonine at position 789$^{6.43}$. The activity was normalized to that of the mock-transfected membranes without L-AP4. The regression line is shown by *dashed line*. *b*, effects on initial rates of the G_o activation abilities by replacement of Thr-789$^{6.43}$ with amino acids smaller than threonine. Experiments were performed with or without 1 mM L-AP4 (*black* and *white bars*, respectively). The activities were normalized to that of mock-transfected membranes. *c*, effects on initial rates of the G_o activation abilities by replacement of Thr-789$^{6.43}$ with amino acids larger than threonine. Experiments were performed with or without 1 mM L-AP4 (*black* and *white bars*, respectively). All of the data are expressed as mean ± S.D. (*error bars*) of more than two independent experiments done in duplicate. * indicates a significant elevation of constitutive activity relative to wild type ($p < 0.05$; Student's *t* test, two-tailed). ** indicates a significant elevation of L-AP4-dependent activity relative to wild type ($p < 0.05$; Student's *t* test, two-tailed). # indicates a significant decrease of L-AP4-dependent activity relative to its constitutive activity ($p < 0.05$; Student's *t* test, two-tailed).

the space between helices VI and VII to avoid a steric hindrance with Tyr-834$^{7.48}$ only in the active state (Fig. 4, *a*, *b*, *e*, and *f*); that is, the mutations T789Y/F$^{6.43}$ stabilize the active state rather than the resting state. This is especially prominent in T789Y$^{6.43}$, as the hydroxyl group of Tyr-789$^{6.43}$ and the backbone carbonyl oxygen of Gly-831$^{7.45}$ were located within 2.9 Å, which would be close enough for hydrogen bonding (*dashed line* in Fig. 4*e*). We speculated that the unique phenotype of T789Y$^{6.43}$ originates from the specific hydrogen bond, which is absent in other mutants. If so, an additional alanine mutation at Gly-831$^{7.45}$ would break the hydrogen bond as shown in Fig. 4*h*. Therefore, the double mutant G831A$^{7.45}$/T789Y$^{6.43}$ should show L-AP4-induced elevation of the activity similar to the other mutants.

Identification of the Interacting Site with T789Y$^{6.43}$—Next, to verify the specific interaction between helices VI and VII speculated from the above mentioned homology modeling, we constructed a series of 15 double mutants combining T789Y$^{6.43}$ with alanine (serine) mutations at position 826$^{7.40}$–840$^{7.54}$ in helix VII. The expression levels of all mutants except for L830A$^{7.44}$/T789Y$^{6.43}$ and L833A$^{7.47}$/T789Y$^{6.43}$ were >60% of wild type (Table 1). Among these 13 double mutants, G831A$^{7.45}$/T789Y$^{6.43}$ clearly showed the rescued wild-type-like phenotype. G831A$^{7.45}$/T789Y$^{6.43}$ significantly elevated the activity in an L-AP4-dependent manner, in contrast with T789Y$^{6.43}$ and other several double mutants (Fig. 5*a*). Moreover, the mutation G831A$^{7.45}$ also suppressed the high constitutive activity of T789Y$^{6.43}$ (Fig. 5*b*). These results strongly suggested that the unique phenotype of T789Y$^{6.43}$ is due to the interaction between Tyr-789$^{6.43}$ and Gly-831$^{7.45}$ as predicted by our model.

The homology model also predicted that several residues in the cytoplasmic side of Gly-831$^{7.45}$, including *X*PK*X*Y motif, in helix VII were not within range to interact directly with Thr-789$^{6.43}$. However, alanine mutations into these positions combined with T789Y$^{6.43}$ also abrogated the phenotype of T789Y$^{6.43}$; that is, alanine mutations into five positions

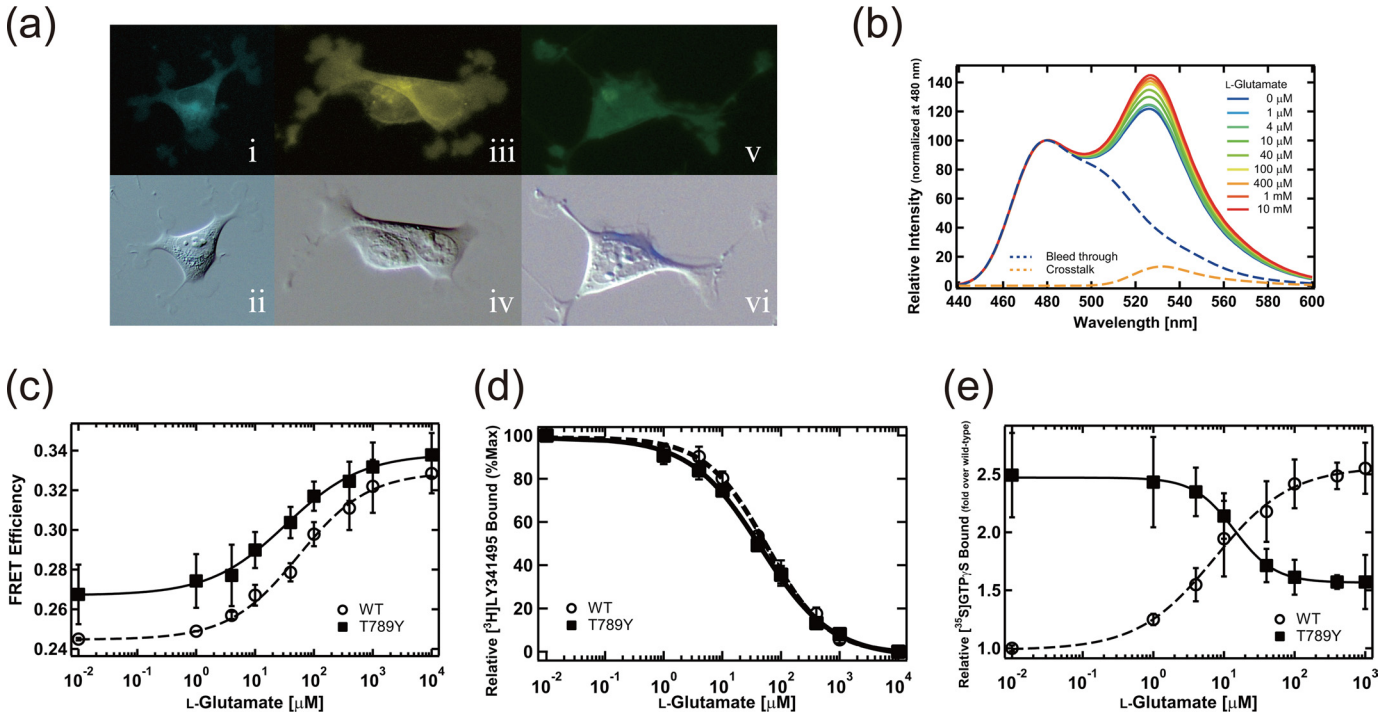

FIGURE 3. **Comparison between a dimeric rearrangement and a change in G protein activation ability of T789Y$^{6.43}$ mutant.** *a*, fluorescence and difference interference contrast images of HEK293 cells expressing Cerulean-fused T789Y$^{6.43}$ (*i* and *ii*), Venus-fused T789Y$^{6.43}$ (*iii* and *iv*), and both of them (*v* and *vi*). The fluorescence images (*i*, *iii*, and *v*) are colored *cyan*, *yellow*, and *green*, respectively. *b*, emission spectra from the HEK293 cell membrane preparation containing Celurean- and Venus-fused T789Y$^{6.43}$ heterodimer. The membrane preparation was excited at 433 nm in 0, 1, 4, 10, 40, 100, and 400 μM, 1 mM, and 10 mM L-glutamate. Bleed-through shows the emission spectrum of Cerulean. All the spectra except for Cross-talk were normalized by the fluorescence intensity at 480 nm. Cross-talk shows the emission spectrum of Venus in the sample directly excited at 433 nm, which can be calculated as previously reported (13). *c*, glutamate-dependent changes of FRET efficiency of Celurean- and Venus-fused wild type (*open circles*) and T789Y$^{6.43}$ (*filled squares*). *d*, displacement by glutamate of [^{3}H]LY341495 binding to the membrane preparation co-expressing Cerulean- and Venus-fused wild type (*open circles*) and T789Y$^{6.43}$ (*filled squares*). *e*, glutamate-dependent changes of G protein activation abilities of wild type (*open circles*) and T789Y (*filled squares*). The EC_{50} (or IC_{50}) values (wild type, 7.9 $\pm$ 4.7 μM; T789Y$^{6.43}$, 14 $\pm$ 9.8 μM) were calculated from the respective curves. Results were normalized to the constitutive activity of wild type. All data are expressed as mean $\pm$ S.D. (*error bars*) of more than three independent experiments.

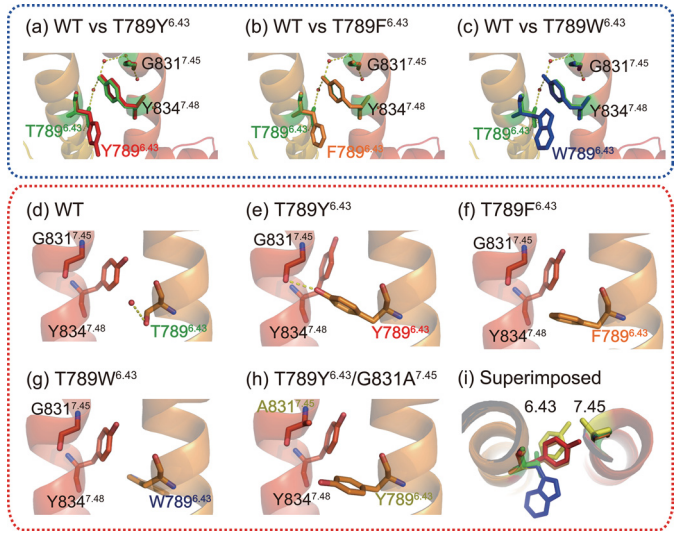

FIGURE 4. **Homology models of mGluR8 mutants.** *a–c*, *blue dashed frame* shows homology models of T789Y$^{6.43}$ (*a*), T789F$^{6.43}$ (*b*), and T789W$^{6.43}$ (*c*) based on the resting state of bovine rhodopsin (1U19) compared with that of wild type. Helices VI and VII are represented as *ribbons*. Highlighted residues correspond to wild-type (*green*) and mutants (*red*, *yellow*, or *blue*). A water-mediated HBN in wild type is indicated by *yellow dashed lines*. *d–h*, *red dashed frame* shows homology models of T789Y$^{6.43}$ (*e*), T789F$^{6.43}$ (*f*), T789W$^{6.43}$ (*g*), and G831A$^{7.45}$/T789Y$^{6.43}$ (*h*) based on the active state of bovine rhodopsin (3PXO) compared with wild type (*d*). Possible hydrogen bonds are indicated by *yellow dashed lines*. *i*, superimposed view of all the models shown in *d–h*. The models were superimposed by using cealign command in PyMOL (26).

(Y834A$^{7.48}$, P836A$^{7.50}$, K837A$^{7.51}$, Y839A$^{7.53}$, and I840A$^{7.54}$) combined with T789Y$^{6.43}$ resulted in L-AP4-induced increase or less reduction of the activity (Fig. 5*a*). In addition, among these double mutants, four mutants except for Y834A$^{7.48}$/T789Y$^{6.43}$ showed suppression of the constitutive activity (Fig. 5*b*). These results suggest that the microenvironment around T789Y$^{6.43}$ is also structurally linked with the cytoplasmic side of helix VII near the *X*PK*X*Y motif in an indirect manner.

We also performed the analysis of single alanine mutations on helix VII. The expression level was severely reduced in L830A$^{7.44}$ and L833A$^{7.47}$, indicating that the low expression level of the double mutants, L830A$^{7.44}$/T789Y$^{6.43}$ and L833A$^{7.47}$/T789Y$^{6.43}$, was attributable to the single mutations in helix VII (Table 1). In the GTPγS binding assay, no mutants showed significant elevation of the constitutive activity (Fig. 5*c*). However, the mutation K837A$^{7.51}$ in the *X*PK*X*Y motif dramatically reduced an L-AP4-dependent activity, suggesting that this residue plays an essential role for the formation of the active state.

DISCUSSION

Positional Relationship between Helices VI and VII within a Protomer Determines the Activation of mGluR—In the last 15 years, growing evidence has demonstrated that the dimeric rearrangement of TMDs following the ligand-induced dimeric relocation of extracellular domains triggers the activation of

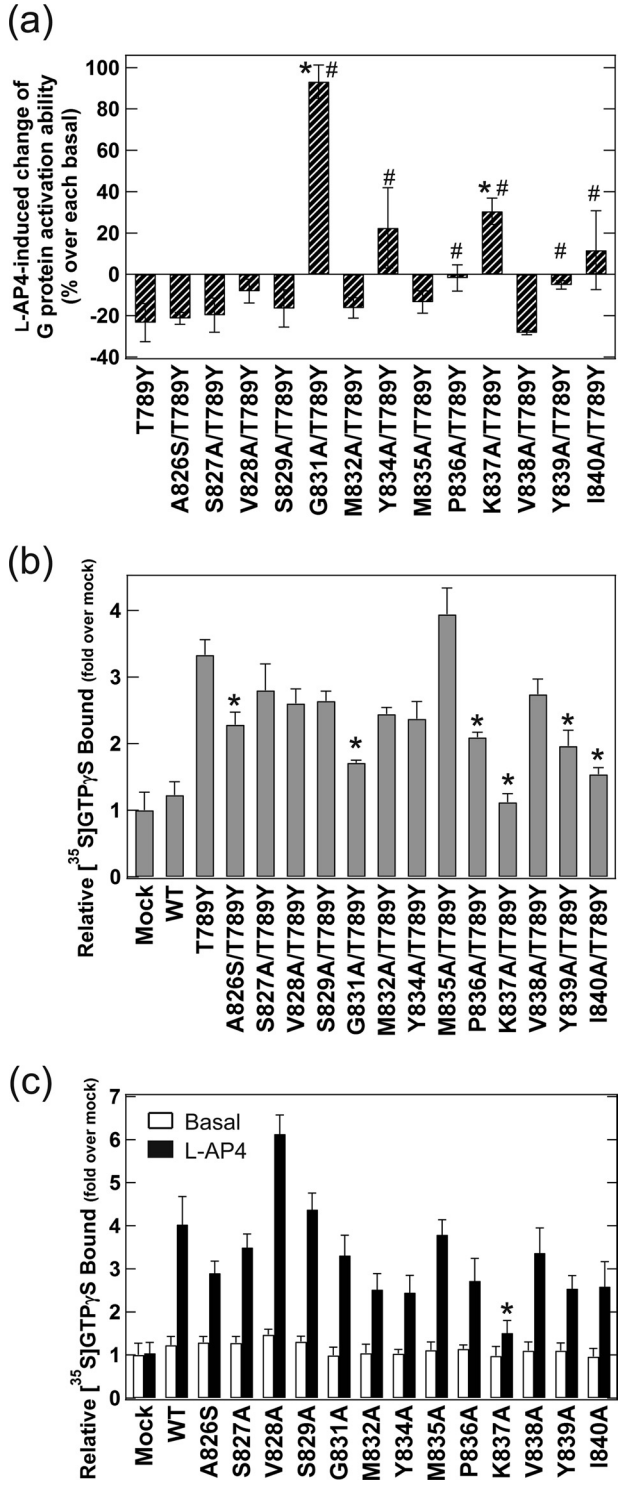

FIGURE 5. **Analyses of a series of double mutants of T789Y$^{6.43}$ and mutations on helix VII.** *a*, L-AP4-induced change of G protein activation ability. Data are expressed as percentage of respective G protein activation abilities without L-AP4. * indicates a significant increase of the activity in an L-AP4-dependent manner, and # indicates a significant change of the activity compared with T789Y$^{6.43}$ ($p < 0.05$; Student's *t* test, two-tailed). *b*, initial rates of G_o activation abilities of double mutants without L-AP4. * indicates a significant decrease of constitutive activity compared with that of T789Y$^{6.43}$ ($p < 0.01$; Student's *t* test, two-tailed). *c*, initial rates of G_o activation abilities of wild type and single mutants on helix VII of mGluR8. Several data in *c* were already published in our previous study (7). Experiments were performed with or without 1 mM L-AP4 (black and white bars, respectively). The activities were normalized to that of mock-transfected membranes. * indicates a significant decrease of L-AP4-dependent activity compared with that of wild-type ($p < 0.01$; Student's *t* test, two-tailed). All the data are expressed as mean ± S.D. (*error bars*) of more than two independent experiments done in duplicate.

family 3 GPCRs (9–14). However, it is unclear what occurs within each TMD after the dimeric rearrangement for the efficient G protein activation. In the present study, we revealed that reorganization of the HBN between helices VI and VII in each TMD of dimer, similar to family 1 GPCRs, is a major determinant of the activation of mGluR by using homology modeling and comprehensive mutation analysis. Namely, the shift between the resting and active states of the receptor primarily depends on the conformation of TMD within each protomer, which should be tightly linked to the dimeric arrangement of TMDs via the dimeric interface.

The activation of GPCR is often explained by a theoretical energy landscape based on a simple two-state model (29, 30). Here we apply the energy landscape to discuss what occurs in the mutants (Fig. 6). In the wild type without ligand, the resting state is stabilized by the proper HBN between helices VI and VII (Figs. 1*a* and 6*a*). We observed a significant correlation between constitutive activity and the side chain volume at position 789$^{6.43}$ (Fig. 2*a*). Therefore, in the Thr-789$^{6.43}$ mutants, large volume residues destabilized the resting state and stabilized the active state as shown in Fig. 4 (*dashed lines* in Fig. 6). The formation of the active state is accompanied by a relatively large space opening around Thr-789$^{6.43}$ between helices VI and VII, although not large enough to accommodate a tryptophan residue (Fig. 4, *g* and *i*). Thus, we speculated that the mutation T789W$^{6.43}$ did not stabilize the resting or active state but fell into a deactivated state (Fig. 6*c*), where the space between helices VI and VII might be abnormally expanded.

Agonist-induced dimeric rearrangement in T789Y$^{6.43}$ was indistinguishable from that of the wild type (13). In wild-type mGluR8, reorganization of the dimeric interface would induce conformational changes within each protomer including widening of the space between helices VI and VII (Figs. 1 and 6*a*). However, in T789Y$^{6.43}$, the space between helices VI and VII was already widened by the interaction between Tyr-789$^{6.43}$ and Gly-831$^{7.45}$ in the absence of a ligand (Fig. 4*e*). Thus, the ligand-induced dimeric rearrangement similar to wild type would further widen the space between helices VI and VII resulting in a deactivated state similar to T789W$^{6.43}$ (Fig. 6*b*).

Similarity and Difference between XPKXY Motif and NPXXY Motif—In the present study, we identified an indirect interaction between T789Y$^{6.43}$ and highly conserved *X*PK*X*Y motif in helix VII of family 3 GPCRs (Fig. 5). The *X*PK*X*Y motif has been considered as a key motif equivalent to the well characterized NP*XX*Y motif in family 1 GPCRs (27). In the case of glycoprotein hormone receptor, Thr$^{6.43}$ and Asp$^{6.44}$ interact mainly with Asn$^{7.49}$ in the NP*XX*Y motif to keep the receptor inactive (31, 32), and naturally occurring constitutively active mutations at these loci cause genetic disorders such as hyperfunctioning thyroid adenoma and familial male-limited precocious puberty (6). Moreover, the recent crystal structure of constitutively active mutant M257Y$^{6.40}$ of rhodopsin showed that elevation of the basal activity originated from the formation of specific interactions among helices III, V, VI, and VII including M257Y$^{6.40}$ and

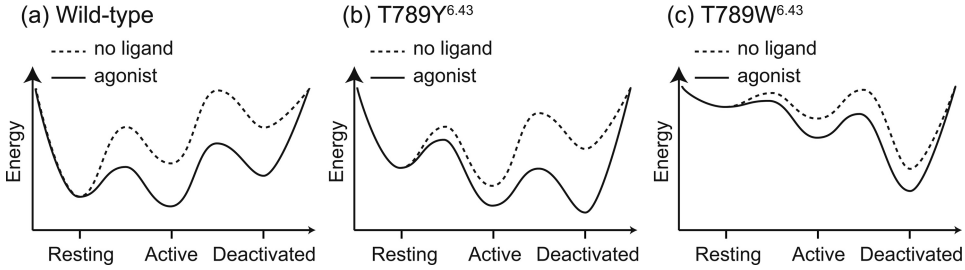

FIGURE 6. **Theoretical energy landscapes of wild type and mutants of mGluR8.** *a*, conformational states of wild-type mGluR8 with or without agonist (*solid* or *dashed line*, respectively). Binding of an agonist lowers the energy barrier and decreases the potential energy of the active state relative to the resting state. *b*, conformational states of T789Y$^{6.43}$ mutant. The mutation increases the potential energy of the resting state relative to the active state. Binding of an agonist lowers the energy barrier and decreases the potential energy of the deactivated state relative to the active state. *c*, conformational states of T789W$^{6.43}$ mutant. The mutation increases the potential energy of both the resting and active states relative to the deactivated state.

Tyr-306$^{7.53}$ in NP*XX*Y motif (33). These cases are quite similar to the present study in that a mutation-induced change of the HBN between helices VI and VII including *X*PK*X*Y or NP*XX*Y motif stabilized the active state instead of the resting state.

Additionally, the present study revealed the importance of Lys-837$^{7.51}$ in *X*PK*X*Y motif for activation of mGluR (Fig. 5), which is specifically conserved in family 3 GPCRs. The homology modeling of mGluR8 shows that Lys-837$^{7.51}$ is oriented toward the outer side of the helical bundles in the cytoplasmic end of helix VII (Fig. 1). Further mutational analysis at position 837$^{7.51}$ will clarify the specific role of Lys-837$^{7.51}$.

CONCLUSION

Why can all GPCRs activate the G protein even though their sequence similarity is very low? This is a fundamental question to be solved. Here we showed that a water-mediated HBN between helices VI and VII stabilizes the resting state of mGluR, similar to family 1 GPCRs. These results suggest that receptors are similarly regulated by a HBN despite their apparent differences. A homology model based on an alignment with low sequence similarity should be skeptically evaluated. However, experimental validation of such homology models can provide important information about the common structural elements that cannot be revealed by simple amino acid sequence alignment.

The present study revealed that the activation of mGluR is primarily induced by conformational changes within each protomer of dimer similar to family 1 GPCRs. However, the molecular mechanism that drives the conformational changes within each TMD may be different between family 1 and family 3 GPCRs. In many family 1 GPCRs, ligand binding to TMD and/or the extracellular loops leads directly to conformational changes in helical bundles irrespective of oligomerization. In contrast, in family 3 GPCRs, ligand binding to a large extracellular domain induces the reorganization of the dimeric interface of TMDs, which drives the helical movement within each protomer (14). Recently, growing evidence has suggested that allosteric modulation via dimerization can be observed in many family 1 GPCRs (34). In family 3 GPCRs, many allosteric modulators directly bind to the TMD and regulate the helical movement (35). Taken together, it can be said that activity modulation by both ligand binding to the TMD and by dimerization is a common feature in family 1 and family 3 GPCRs. However, the modulation of the dimeric interface is considered to be "an allosteric effect" in family 1 GPCRs and "an orthosteric effect" in family 3 GPCRs. Further research on family 3 GPCRs will further our understanding of the functional regulation by the dimerization of GPCRs.

Acknowledgments—We thank Prof. J. Nathans for the HEK293S cell line, Prof. R. S. Molday for the Rho 1D4-producing hybridoma, Prof. H. Niwa for pCAGGS vector, Prof. D. W. Piston for the clone of mCerulean, and Prof. A. Miyawaki for the clone of Venus. We also thank Dr. Y. Imamoto for very helpful discussions and Dr. T. Matsuyama for a critical reading of our manuscript and invaluable comments.

REFERENCES

1. Vroling, B., Sanders, M., Baakman, C., Borrmann, A., Verhoeven, S., Klomp, J., Oliveira, L., de Vlieg, J., and Vriend, G. (2011) GPCRDB: information system for G protein-coupled receptors. *Nucleic Acids Res.* **39,** D309–319
2. Choe, H. W., Kim, Y. J., Park, J. H., Morizumi, T., Pai, E. F., Krauss, N., Hofmann, K. P., Scheerer, P., and Ernst, O. P. (2011) Crystal structure of metarhodopsin II. *Nature* **471,** 651–655
3. Rasmussen, S. G., DeVree, B. T., Zou, Y., Kruse, A. C., Chung, K. Y., Kobilka, T. S., Thian, F. S., Chae, P. S., Pardon, E., Calinski, D., Mathiesen, J. M., Shah, S. T., Lyons, J. A., Caffrey, M., Gellman, S. H., Steyaert, J., Skiniotis, G., Weis, W. I., Sunahara, R. K., and Kobilka, B. K. (2011) Crystal structure of the β2 adrenergic receptor-Gs protein complex. *Nature* **477,** 549–555
4. Okada, T., Fujiyoshi, Y., Silow, M., Navarro, J., Landau, E. M., and Shichida, Y. (2002) Functional role of internal water molecules in rhodopsin revealed by x-ray crystallography. *Proc. Natl. Acad. Sci. U.S.A.* **99,** 5982–5987
5. Angel, T. E., Chance, M. R., and Palczewski, K. (2009) Conserved waters mediate structural and functional activation of family A (rhodopsin-like) G protein-coupled receptors. *Proc. Natl. Acad. Sci. U.S.A.* **106,** 8555–8560
6. Smit, M. J., Vischer, H. F., Bakker, R. A., Jongejan, A., Timmerman, H., Pardo, L., and Leurs, R. (2007) Pharmacogenomic and structural analysis of constitutive g protein-coupled receptor activity. *Annu. Rev. Pharmacol. Toxicol.* **47,** 53–87
7. Yanagawa, M., Yamashita, T., and Shichida, Y. (2009) Activation switch in the transmembrane domain of metabotropic glutamate receptor. *Mol. Pharmacol.* **76,** 201–207
8. Ballesteros, J., and Weinstein, H. (1995) Integrated methods for the construction of three-dimensional models and computational probing of structure-function relations in G protein-coupled receptors. *Methods Neurosci.* **25,** 366–428
9. Kunishima, N., Shimada, Y., Tsuji, Y., Sato, T., Yamamoto, M., Kumasaka, T., Nakanishi, S., Jingami, H., and Morikawa, K. (2000) Structural basis of glutamate recognition by a dimeric metabotropic glutamate receptor. *Nature* **407,** 971–977
10. Muto, T., Tsuchiya, D., Morikawa, K., and Jingami, H. (2007) Structures of

the extracellular regions of the group II/III metabotropic glutamate receptors. *Proc. Natl. Acad. Sci. U.S.A.* **104,** 3759–3764
11. Huang, S., Cao, J., Jiang, M., Labesse, G., Liu, J., Pin, J. P., and Rondard, P. (2011) Interdomain movements in metabotropic glutamate receptor activation. *Proc. Natl. Acad. Sci. U.S.A.* **108,** 15480–15485
12. Tateyama, M., Abe, H., Nakata, H., Saito, O., and Kubo, Y. (2004) Ligand-induced rearrangement of the dimeric metabotropic glutamate receptor 1α. *Nat. Struct. Mol. Biol.* **11,** 637–642
13. Yanagawa, M., Yamashita, T., and Shichida, Y. (2011) Comparative fluorescence resonance energy transfer analysis of metabotropic glutamate receptors: implications about the dimeric arrangement and rearrangement upon ligand bindings. *J. Biol. Chem.* **286,** 22971–22981
14. Hlavackova, V., Zabel, U., Frankova, D., Bätz, J., Hoffmann, C., Prezeau, L., Pin, J. P., Blahos, J., and Lohse, M. J. (2012) Sequential inter- and intrasubunit rearrangements during activation of dimeric metabotropic glutamate receptor 1. *Sci. Signal.* **5,** ra59
15. Rizzo, M. A., Springer, G. H., Granada, B., and Piston, D. W. (2004) An improved cyan fluorescent protein variant useful for FRET. *Nat. Biotechnol.* **22,** 445–449
16. Nagai, T., Ibata, K., Park, E. S., Kubota, M., Mikoshiba, K., and Miyawaki, A. (2002) A variant of yellow fluorescent protein with fast and efficient maturation for cell-biological applications. *Nat. Biotechnol.* **20,** 87–90
17. Niwa, H., Yamamura, K., and Miyazaki, J. (1991) Efficient selection for high-expression transfectants with a novel eukaryotic vector. *Gene* **108,** 193–199
18. Yamashita, T., Terakita, A., Kai, T., and Shichida, Y. (2008) Conformational change of the transmembrane helices II and IV of metabotropic glutamate receptor involved in G protein activation. *J. Neurochem.* **106,** 850–859
19. Eswar, N., Webb, B., Marti-Renom, M. A., Madhusudhan, M. S., Eramian, D., Shen, M. Y., Pieper, U., and Sali, A. (2006) Comparative protein structure modeling using Modeller. *Curr. Protoc. Bioinformatics* **Chapter 5,** Unit 5.6
20. Okada, T., Sugihara, M., Bondar, A. N., Elstner, M., Entel, P., and Buss, V. (2004) The retinal conformation and its environment in rhodopsin in light of a new 2.2 Å crystal structure. *J. Mol. Biol.* **342,** 571–583
21. Malherbe, P., Kratochwil, N., Knoflach, F., Zenner, M. T., Kew, J. N., Kratzeisen, C., Maerki, H. P., Adam, G., and Mutel, V. (2003) Mutational analysis and molecular modeling of the allosteric binding site of a novel, selective, noncompetitive antagonist of the metabotropic glutamate 1 receptor. *J. Biol. Chem.* **278,** 8340–8347
22. Malherbe, P., Kratochwil, N., Zenner, M. T., Piussi, J., Diener, C., Kratzeisen, C., Fischer, C., and Porter, R. H. (2003) Mutational analysis and molecular modeling of the binding pocket of the metabotropic glutamate 5 receptor negative modulator 2-methyl-6-(phenylethynyl)-pyridine. *Mol. Pharmacol.* **64,** 823–832
23. Petrel, C., Kessler, A., Maslah, F., Dauban, P., Dodd, R. H., Rognan, D., and Ruat, M. (2003) Modeling and mutagenesis of the binding site of Calhex 231, a novel negative allosteric modulator of the extracellular Ca^{2+}-sensing receptor. *J. Biol. Chem.* **278,** 49487–49494
24. Miedlich, S. U., Gama, L., Seuwen, K., Wolf, R. M., and Breitwieser, G. E. (2004) Homology modeling of the transmembrane domain of the human calcium sensing receptor and localization of an allosteric binding site. *J. Biol. Chem.* **279,** 7254–7263
25. Bruno, A., Costantino, G., de Fabritiis, G., Pastor, M., and Selent, J. (2012) Membrane-sensitive conformational states of helix 8 in the metabotropic Glu2 receptor, a class C GPCR. *PLoS One* **7,** e42023
26. Grell, L., Parkin, C., Slatest, L., and Craig, P. A. (2006) EZ-Viz, a tool for simplifying molecular viewing in PyMOL. *Biochem. Mol. Biol. Educ.* **34,** 402–407
27. Pin, J. P., Galvez, T., and Prézeau, L. (2003) Evolution, structure, and activation mechanism of family 3/C G-protein-coupled receptors. *Pharmacol. Ther.* **98,** 325–354
28. Binet, V., Duthey, B., Lecaillon, J., Vol, C., Quoyer, J., Labesse, G., Pin, J. P., and Prézeau, L. (2007) Common structural requirements for heptahelical domain function in class A and class C G protein-coupled receptors. *J. Biol. Chem.* **282,** 12154–12163
29. Kobilka, B. K., and Deupi, X. (2007) Conformational complexity of G-protein-coupled receptors. *Trends Pharmacol. Sci.* **28,** 397–406
30. Deupi, X., and Kobilka, B. K. (2010) Energy landscapes as a tool to integrate GPCR structure, dynamics, and function. *Physiology* **25,** 293–303
31. Govaerts, C., Lefort, A., Costagliola, S., Wodak, S. J., Ballesteros, J. A., Van Sande, J., Pardo, L., and Vassart, G. (2001) A conserved Asn in transmembrane helix 7 is an on/off switch in the activation of the thyrotropin receptor. *J. Biol. Chem.* **276,** 22991–22999
32. Urizar, E., Claeysen, S., Deupí, X., Govaerts, C., Costagliola, S., Vassart, G., and Pardo, L. (2005) An activation switch in the rhodopsin family of G protein-coupled receptors: the thyrotropin receptor. *J. Biol. Chem.* **280,** 17135–17141
33. Deupi, X., Edwards, P., Singhal, A., Nickle, B., Oprian, D., Schertler, G., and Standfuss, J. (2012) Stabilized G protein binding site in the structure of constitutively active metarhodopsin-II. *Proc. Natl. Acad. Sci. U.S.A.* **109,** 119–124
34. Khelashvili, G., Dorff, K., Shan, J., Camacho-Artacho, M., Skrabanek, L., Vroling, B., Bouvier, M., Devi, L. A., George, S. R., Javitch, J. A., Lohse, M. J., Milligan, G., Neubig, R. R., Palczewski, K., Parmentier, M., Pin, J. P., Vriend, G., Campagne, F., and Filizola, M. (2010) GPCR-OKB: the G protein-coupled receptor oligomer knowledge base. *Bioinformatics* **26,** 1804–1805
35. Urwyler, S. (2011) Allosteric modulation of family C G-protein-coupled receptors: from molecular insights to therapeutic perspectives. *Pharmacol. Rev.* **63,** 59–126